Articles in PresS. J Appl Physiol (May 2, 2013). doi:10.1152/japplphysiol.00662.2012

Analysis of Patient-specific Surgical Ventricular Restoration - Importance of an Ellipsoidal Left Ventricular Geometry for Diastolic and Systolic Function

Lik Chuan Lee[1,2], Jonathan F. Wenk[3], Liang Zhong[4], Doron Klepach[1,2], Zhihong Zhang[1], Liang Ge[1,2], Mark B. Ratcliffe[1,2], Tarek I. Zohdi[5], Edward Hsu[6], Jose L. Navia[7], Ghassan S. Kassab[8] and Julius M. Guccione[1,2]

Department of Surgery[1] and Bioengineering[2], University of California, San Francisco, CA; Department of Mechanical Engineering and Surgery University of Kentucky, Lexington, KY [3]; Department of Cardiology, National Heart Centre Singapore[4]; Department of Mechanical Engineering, University of California, Berkeley[5]; Department of Bioengineering, The University of Utah[6]; Cleveland Clinic[7]; Department of Biomedical Engineering, Indiana University –Purdue University Indianapolis [8]

Author Contributions:

Lik Chuan, Lee:	Mathematical modeling, result analysis, manuscript writing.
Jonathan F. Wenk:	Mathematical modeling.
Liang Zhong:	Manuscript editing, Data collection.
Doron Kepach:	Mathematical modeling.
Zhang Zhihong:	Mathematical modeling.
Liang Ge:	Result analysis.
Mark B. Ratcliffe:	Result analysis.
Edward Hsu:	Data collection.
Jose L. Navia:	Data collection.
Tarek Zohdi:	Manuscript editing.
Ghassan S. Kassab:	Manuscript editing, result analysis.
Julius M. Guccione:	Manuscript editing, result analysis.

Running head: Analysis of patient-specific SVR

*Corresponding Author:
Julius M. Guccione
UCSF/VA Medical Center (112D)
4150 Clement Street
San Francisco, CA 94121
Phone: 415-221-4810
Fax: 415-750-2181
Email: julius.guccione@yahoo.com

Summary

Surgical ventricular restoration (SVR) is a procedure designed to treat heart failure by surgically excluding infarcted tissues from the dilated failing left ventricle. To elucidate and predict the effects of geometrical changes from SVR on cardiac function, we created patient-specific mathematical (finite element) left ventricular models before and after surgery using untagged magnetic resonance images. Our results predict that the post-surgical improvement in systolic function was compromised by a decrease in diastolic distensibility in patients. These two conflicting effects typically manifested as a more depressed Starling relationship (stroke volume vs. end-diastolic pressure) after surgery. By simulating a restoration of the left ventricle back to its measured baseline sphericity, we show that both diastolic and systolic function improved. This result confirms that the increase in left ventricular sphericity commonly observed after SVR (endoventricular circular patch plasty) has a negative impact and contributes partly to the depressed Starling relationship. On the other hand, peak myofiber stress was reduced substantially (by 50%) after SVR and the resultant left ventricular myofiber stress distribution became more uniform. This significant reduction in myofiber stress after SVR may help reduce adverse remodeling of the left ventricle. These results are consistent with the speculation proposed in the STICH trial (20) for the neutral outcome, that "the lack of benefit seen with surgical ventricular reconstruction is that benefits anticipated from surgical reduction of left ventricular volume (reduced wall stress and improvement in systolic function) are counter-balanced by a reduction in diastolic distensibility."

Keywords: Myocardial infarction, Surgical ventricular restoration, Finite element modeling, Coronary artery bypass grafting.

Word Count: 243

Introduction

Surgical ventricular restoration (SVR) is a procedure designed to treat heart failure by surgically excluding infarcted tissues from the dilated failing left ventricle (LV). The aim of this treatment is to neutralize the negative physiologic effects of dysfunctional regions in the left ventricular wall. The "Surgical Treatment for Ischemic Heart Failure" (STICH) trial was conducted to assess the effectiveness of SVR (35). One of the two components of the trial was to determine whether adding SVR to Coronary Artery Bypass Grafting (CABG) would decrease the rate of death or hospitalization for cardiac causes more than CABG alone. The clinical findings led the authors to conclude that adding SVR to CABG reduces the LV volume compared to CABG alone, but this reduction is not associated with a greater improvement in symptoms, exercise tolerance or a reduction in the rate of death or hospitalization for cardiac causes. One speculation for these findings was that the benefits anticipated from the surgical reduction of LV volume were counterbalanced by a reduction in diastolic distensibility (21).

Although the STICH trial concluded that SVR, when performed with CABG, adds no benefits to the patient, this conclusion remains controversial (7, 8, 26). Clinical studies have shown that SVR did benefit patients who had myocardial infarction (3, 4, 8, 19, 24, 28) and both the European Society of Cardiology and European Association for Cardio-Thoracic Surgery recommend SVR if LV volume is measured, scar is identified and surgery is performed in centers with a high level of surgical expertise (37). Conversely, clinical studies have also shown that stroke volume (SV) decreased after SVR (13, 22, 34, 39), and the decrease in size of the LV after SVR can be accompanied by an increase in LV sphericity (12, 23, 39). This post-surgical increase in LV sphericity was believed to impair diastolic function (27). On the other hand, the supposedly lower ventricular wall stress (based on Laplace's law) resulting from a reduction in LV size after SVR should in principle benefit patients by reducing myocardial oxygen demand (30). These conflicting effects of SVR contribute, in part, to the gap in our understanding as to why patients who underwent SVR did not always receive the benefits from the supposedly lower wall

stress. Bridging this gap requires accurate quantification of the local myofiber stress, which at present, can be determined only through patient-specific mathematical modeling (38).

Patient-specific mathematical modeling of the effects of SVR is largely lacking and is, at best, overly simplified. Many mathematical analyses of SVR have been conducted based on animal LV models. For example, a mathematical model of the sheep LV by Dang et al. (10) was used to study the effects of SVR alone (without CABG) on diastolic distensibility, end-systolic elastance, the Starling relationship (SV versus end-diastolic pressure) and regional myofiber stress distribution. Their results suggest that when compared to the remote region, SVR reduces myofiber stress in the akinetic infarct and infarct borderzone. They also found that the Starling relationship was depressed after SVR. However, this result is based on a sheep LV and did not address the increase in sphericity of the post-surgical LV commonly found in patients. On the other hand, a recent analysis of the patient-specific effects of SVR found it reduced the LV bulk wall stress and improved the LV systolic function (40). That analysis was based on a local balance of forces, however, and cannot account for myofiber orientation or predict myofiber stress distribution within the LV (38).

To elucidate the functional effects resulting from the geometrical change found in the LV after SVR, we performed the first mathematical analysis on the effects of SVR using patient-specific finite element (FE) LV models. These models were created using untagged magnetic resonance (MR) images from the same set of patient data described in Zhong et al. (39).

Material and Methods

Acquisition of magnetic resonance images

The method used for magnetic resonance imaging (MRI) is detailed in Zhong et al. (40). All procedures in patients were approved by our institutional review board and patient consents were obtained. The MR images were de-identified. Images were obtained one to two weeks before surgery and one to two weeks after surgery with a 1.5-T MRI scanner (Siemens Somatom, Erlangen, Germany). These images were

segmented interactively by outlining the LV endocardial and epicardial borders (excluding papillary muscles and trabeculation) using CMRtools. Then, the set of LV contour points derived from the segmentation process was triangulated using Rapidform© (INUS Technology, Inc) to reconstruct the three-dimensional (3D) LV epicardial and endocardial surfaces. End-diastolic (ED) and end-systolic (ES) cardiac phases were determined by visualizing the mitral valve and the aortic valve closure.

Finite element modeling

We used the FE method to analyze the effects of surgery (CABG + SVR) in 12 patients (randomly selected from a cohort of 40 patients). In each patient, the SVR procedure was performed using the endoventricular circular patch plasty technique. Three of these 12 patients had concomitant mitral regurgitation and underwent mitral valve repair surgery by means of restrictive mitral annuloplasty. A multivariable general linear model analysis was performed on this patient cohort and did not detect any differences between patients who received mitral valve repair surgery (MVR) and patients who did not receive MVR (39). Finite element models of the LV were created by projecting a mesh between the 3D endocardial and the 3D epicardial surface reconstructed from the acquired MR images (33) at early diastole (Truegrid, XYZ Scientific Applications, Inc., Livermore, CA). The mesh in each LV model consisted of between 2000 to 4000 trilinear 8-noded brick elements.

In the pre–surgery models, two distinct material regions were defined: the transmural infarct region and the remote region. The infarct region was defined as the region without any relative wall motion; i.e., akinesia. The remote-infarct boundary was identified by overlapping the ED and the ES endocardial surface. Then, this boundary was projected transmurally onto the epicardial surface. In the post-surgery models, the entire LV was assumed to be composed of a single material as there were no significant overlapping regions. Residual stress was not included in the post-surgery LV models because the effects were found to be negligible in a previous study (16). Rigid body motion of the LV was suppressed by constraining the base from moving in the longitudinal direction and by constraining the epicardial-basal edge from moving in all directions.

Myofiber angle distribution was assumed to vary transmurally from epicardium to endocardium via a linear transition from -60º to +60º relative to the circumferential direction in all models (16, 29). Also, we have recently obtained unpublished *ex-vivo* diffusion tensor magnetic resonance imaging (DTMRI) fiber angle measurements from 5 explanted human hearts with ischemic heart failure. The myofiber angle was found to vary transmurally from -42.4° (epicardium) to 35.7° (endocardium) on average. To test whether the conclusions of our analysis would be impacted if these new fiber angle data were used, we repeated the analysis on one LV model using these new fiber data.

Because pressure was not measured in the LV, the end-systolic pressure (ESP) was assumed to match the measured systolic blood pressure (SBP) of individual patients. The average SBP of the patients was 121 mmHg pre-surgery and 117 mmHg post-surgery. End-diastolic pressure (EDP) was assumed to be 12 mmHg pre-surgery and post-surgery. The pressure was applied to the LV endocardial surface. To assess the sensitivity of the pressure-volume and Starling relationship to EDP and ESP, we repeated the analysis with EDP at 4 and 20 mmHg and ESP at 90% and 110% of the SBP. The sensitivity of the end-systolic myofiber stress to ESP was also assessed for each case. We note that the estimation of ESP = 0.9 × systolic blood pressure, as was used in many studies; e.g. in (6), falls within the range of ESP used in our sensitivity analysis. Although the sensitivity analysis did not account for inter-individual differences in the LV pressure (especially in EDP), it did confirm that the overall conclusions of this study are not sensitive to the LV pressure assumptions.

Passive and active constitutive laws previously described by Guccione et al. (17, 18) were used in this study (see Appendix A.1). The constitutive laws were implemented with a user-defined material subroutine in LS-DYNA (Livermore Software Technology Corporation, Livermore, CA). Passive stiffness of myocardial tissue was characterized by the material parameter C in the constitutive law. To obtain C in each of the model, we adjusted the C-values so that the predicted LV cavity volume of the FE model matched the measured end-diastolic volume (EDV). In the pre-surgery models, C at infarct (C_I) was set to be ten times stiffer than that in the remote region (C_R) (36). Myocardial

tissue contractility in the active constitutive law was characterized by the material parameter T_{max}, which is the strength of contraction at the longest sarcomere length in the tissue. In the post-surgery FE models, T_{max} was adjusted so that the predicted LV cavity volume matched the measured end-systolic volume (ESV). In the pre-surgery FE models, T_{max} at the infarct (T_{max_I}) and at the remote region (T_{max_R}) were optimized so that: (i) the radial strain was nominally zero at the infarct because changes in wall thickness are minimal in akinesia, and (ii) the predicted LV cavity volume subjected to ESP was within ±1% of the measured ESV. The optimization was implemented using LS-OPT (Livermore Software Technology Corporation, Livermore, CA). The approach of determining active material parameters in the pre-surgery models was adopted from Dang et al. (11), who have used FE models extrapolated from 2D echocardiography to examine akinetic infarcts. Although our models did not physically include any post-surgical implants (e.g. rigid rings, patches), the mechanical effects of these implants were, nevertheless, reflected in the material parameters C and T_{max} as they were calculated based on the MRI-measured LV volumes and LV pressures that are within a physiological range.

Two post-surgery FE models were used to perform a study on the effects of LV sphericity, which was quantified by the short-to-long-axis ratio or sphericity index (SI). The long axis dimension was defined to be the apex to base distance and the short axis dimension was defined to be the maximum epicardial diameter measured at the mid-LV; i.e., half way between apex and base. A large value of SI indicates a more spherical LV, whereas a small value of SI indicates a more ellipsoidal LV. To simulate a change in SI, a downward force was applied at the apical region to elongate the LV and a negative pressure was concurrently applied at the mid-basal endocardial wall to ensure that the LV cavity volume remained constant. Then, the resultant LV geometry was used as the initial "stress-free" configuration to which the same fiber angle distribution was assigned. Because the myocardial material is incompressible, the LV wall mass remained constant after the LV shape was modified. The downward force was not present in subsequent analyses performed on the resultant LV. This force was used purely for modifying

the geometry of the LV. The corresponding post-surgery material parameters C and T_{max} were used in the elongated LV models.

Pressure–volume and Starling relationships

Global LV performance was quantified using the pressure-volume relationship at ED and ES, as well as by the Starling relationship. To obtain the end-diastolic pressure-volume relationship (EDPVR), the FE models were used to predict the LV EDV at different EDP ranging between 0 to 25 mm Hg. Then, the resulting pressure-volume relationship was fitted using an exponential function

$$EDP = A(e^{K_{ED}\cdot(EDV - V_{o,ED})} - 1). \quad (1)$$

In Eq. (1), A, $V_{o,ED}$ and K_{ED} are the fitting parameters. The parameter $V_{o,ED}$ is the LV volume at zero pressure, whereas the parameters K_{ED} and A affect the LV compliance during filling. Diastolic function was quantified using the linear slope of EDPVR at 12mmHg (E_{ED}). An improvement in diastolic function was characterized by a decrease in E_{ED}.

The end-systolic pressure-volume relationship (ESPVR) was obtained from the FE models by simulating the LV at different ESP, ranging from 0 to 140 mmHg. The computed LVESVs were fitted to the corresponding applied ESPs using a linear function (2, 31) as given in the next equation:

$$ESP = E_{ES}(ESV - V_{o,ES}). \quad (2)$$

An improvement in systolic function is characterized by an increase in the end-systolic elastance E_{ES} i.e., the gradient of the linear fit, as well as by a decrease in the volume intersection $V_{o,ES}$ of the ESPVR. The simultaneous improvement of the diastolic and systolic function translates to an improvement in SV and the Starling relationship.

To calculate the Starling relationship, we followed the approach used in Dang et al. (10). The arterial elastance was calculated (for each case) from the measured SV, the measured EDV, the fitted E_{ES} and the volume–intersect $V_{o,ES}$ of the ESPVR using Eq. (3) in Dang et al. (10). Then, the Starling relationship (SV-EDP) was obtained using that same equation by substituting for these values as well as for the computed EDPVR. We note that SV was not compensated in the 3 patients who had concomitant mitral regurgitation and underwent mitral valve repair surgery. In the study on the effects of sphericity, the arterial elastance was kept constant in each of the two groups. We have chosen here to use SV to quantify the LV performance instead of ejection fraction (EF) because EF is not an independent measure of LV performance after SVR (i.e., it is also sensitive to the decrease in EDV after surgery).

Results

Unless otherwise indicated, all results are reported as mean ± standard deviation. Individual results from each patient are shown in the supplemental materials.

Reconstructed left ventricular geometries and hemodynamics measurements

Figure 1a shows a representation of the pre-surgery and post-surgery FE LV model from 12 patients. The remote region is illustrated by the lighter region, and, in the pre–surgery models, the darker region illustrates the infarct. On average, measured EDV decreased by 92.7 ± 31.0 ml (from 269.6 ± 63.5 ml to 176.9 ± 58.0 ml) and measured ESV decreased by 78.7 ± 30.1 ml (from 210.4 ± 62.5 ml to 131.7 ± 63.2 ml) after surgery. The measured heart rate of these patients increased by 6.8 ± 9.5 beats/min after surgery (from 73.0 ± 8.4 beats/min to 79.8 ± 8.4 beats/min) and the corresponding cardiac output decreased by 0.6 ± 1.5 L/min (from 4.3 ± 1.2 L/min and 3.6 ± 1.5 L/min) after surgery. Measured systemic vascular resistance index increased by 620 ± 1890 dyn.s.cm^{-5}.m^{-2} (from 2670 ± 660 dyn.s.cm^{-5}.m^{-2} to 3290 ± 1820 dyn.s.cm^{-5}.m^{-2}) after surgery. We also found that the LV became invariably more spherical after surgery as illustrated in Fig. 1b. On average, SI increased by 30%, from 0.72 ± 0.07 to 0.98 ± 0.11 after surgery.

Predicted global LV performance

Figure 2 shows a representation of the effects of surgery on the ESPVR and EDPVR found in a typical patient. The bounds of the pressure-volume relationship from the sensitivity analysis are also displayed in the figure. We found that ESPVR consistently shifted to the left and became steeper after surgery. On average, the decrease in volume-intersect $V_{o,ES}$ after surgery was 64.1 ± 26.2 ml (from 159.2 ± 51.0 ml to 95.1 ± 51.3 ml), and the end-systolic elastance E_{ES} increased by more than 1.5 times (from 2.40 ± 0.81 mmHg/ml to 3.93 ± 2.20 mmHg/ml). Global systolic function therefore improved after surgery. This result was also insensitive to the choice of ESP. For the range of ESP at 90% - 110% of the SBP, the average values of $V_{o,ES}$ and E_{ES} before surgery fell within 158.4 – 160.0 ml and 2.22 - 2.57 mmHg/ml, respectively. After surgery, the average values of $V_{o,ES}$ and E_{ES} for this range of ESP fell within 94.7 – 95.7 ml and 3.55 - 4.25 mmHg/ml, respectively.

Although global systolic function improved, global diastolic function to worsen after surgery and the LV became less compliant during filling. Specifically, E_{ED} increased from 0.48 ± 0.15 mmHg/ml to 0.82 ± 0.46 mmHg/ml after surgery. For the range of EDP of 4 - 20 mmHg, the average value of E_{ED} before surgery fell within 0.45 - 0.52 mmHg/ml, respectively. After surgery, the average values of E_{ED} for this range of EDP fell within 0.78 - 0.92 mmHg/ml, respectively. Therefore, the decrease in global diastolic function predicted by our mathematical models was also insensitive to the choice of EDP.

These counteracting effects found in the ESPVR and EDPVR typically translated to a more depressed Starling relationship. The predicted Starling relationship remained unchanged in three patients (Fig. 3a), worsened in eight patients (Fig. 3b) and improved only in one (Fig. 3c). Overall, SV decreased from 59.1 ± 18.5 ml to 45.1 ± 19.1 ml, an average drop of 14 ml. Hence, the improvement gained in the systolic function after surgery was negated by a worsening diastolic function in most cases.

Predicted myofiber stress distribution

Figure 4a shows the effect of surgery on the LV regional myofiber stress at end-systole in a representative patient. Before surgery, myofiber stress was highly inhomogeneous in the LV and was significantly elevated at the thin apical region where the infarct resides. After surgery, the decrease in LV size was accompanied by an increase in LV wall thickness, which led to a significant reduction in the peak myofiber stress. As a result, the myofiber stress distribution became more homogeneous after surgery. Figure 4b shows the peak myofiber stress in the LV before and after surgery in all 12 patients. Peak myofiber stress after SVR was substantially reduced in all patients regardless of whether this comparison was made with the peak myofiber stress found in the remote region of the pre-surgery LV or in the entire pre-surgery LV. On average, peak myofiber stress decreased by 50% (from 141.2 ± 45.1 kPa to 70.3 ± 15.0 kPa) when compared to the remote region of the pre-surgery LV.

Predicted effects of left ventricular sphericity

Figure 5 shows the effects of sphericity on the post-surgical LV model from Patient 1. Similar effects were also found in Patient 2 (not shown). Figure 5a shows the geometry of the post-surgical LV as it was "virtually elongated" (from the original post-surgery SI of 0.96 to an SI of 0.67) using the method described in the last paragraph of the section "Finite Element Modeling". The LV cavity volume and the LV wall mass remained constant during this virtual "elongation" process. Figure 5b shows the ESPVR and EDPVR with SI as a parameter. As SI decreased, or equivalently, as the LV became more elongated, it became more compliant and diastolic function improved as a result. For patient 1, E_{ED} decreased moderately by about 6% (from 0.96 to 0.90 mmHg/ml, respectively) with a 30% decrease in SI. Roughly the same percentage of decrease in E_{ED} was also seen in patient 2 when SI decreased from 0.82 to 0.63. Similar to the effects of SI on diastolic function, systolic function also improved slightly as SI decreased. As SI decreased in Patient 1, E_{ES} increased slightly from 4.40 to 4.46 mmHg/ml and $V_{o,ES}$ decreased from 53.1 to 50.6 ml. The same percentage of improvement in systolic function was also found in Patient

2 when SI decreased. The concurrent improvements in systolic and diastolic function were translated into an improvement in the Starling relationship (Fig. 5c). For an EDP between 4 to 20 mmHg, SV increased by about 3.5ml in both patients after a 30% reduction in SI. The diastolic and systolic function and the Starling relationship did not improve after further reduction of SI.

All the above-mentioned results were found to be relatively insensitive to a change in fiber angle distribution based on the repeated analysis (on one patient) using the recently acquired transmural linear variation of fiber angle from -42.4° (epicardium) to 35.7° (endocardium).

Discussion

Effects on stroke volume, systolic and diastolic function

The improvement in systolic function after SVR was compromised by a concurrent decrease in the LV diastolic distensibility. This conclusion is broadly consistent with the speculation offered from the STICH trial (21) and the findings from clinical studies by Tulner et al. (34) and Brinke et al. (5), who observed similar effects of the surgery on EDPVR when invasive pressure-volume measurements were used directly after cardiopulmonary bypass (34) and six months after surgery (5). Specifically, K_{ED} was found to increase from 0.021 ± 0.009 to 0.037 ± 0.021 ml^{-1} after surgery in Tulner et al., and from 0.012 ± 0.003 to 0.023 ± 0.007 ml^{-1} after surgery in Brinke et al. In the clinical study by Brinke et al., end-diastolic elastance E_{ED} (taken at 18 mmHg) was also found to have increased from 0.15 ± 0.08 to 0.24 ± 0.10 mmHg/ml after surgery. Although our prediction of E_{ED} (0.48 ± 0.15 mmHg/ml and 0.82 ± 0.46 mmHg/ml at pre- and post-surgery, respectively) is larger than the measurements by Brinke et al., the percent increase is comparable. In terms of ESPVR, Tulner et al. found that E_{ES} improved from 1.12 ± 0.63 to 1.57 ± 0.55 mmHg/ml, whereas Brinke et al. reported no significant change in E_{ES} (1.2 ± 0.6 mmHg/ml) at six months after surgery. Although these values were also smaller than our prediction (2.40 ± 0.81 mmHg/ml and 3.93 ± 2.20 mmHg/ml before and after surgery), the percent improvement predicted by our mathematical models is comparable to that reported by Tulner et al.

As a result of the counteracting effects of surgery on ESPVR and EDPVR, our results show that the Starling relationship (or SV) was usually more depressed after surgery. This result is consistent with clinical findings (13, 22, 34, 39). The average decrease in SV found from these studies was about 7.5ml (compared to a decrease of 14 ml found here). In the clinical study by Brinke et al. (5), SV improved from 60 ± 17 to 68 ± 13 ml six months after surgery.

Effects of a more ellipsoidal LV

Our results show that the decrease in SV was also accompanied by an increase in SI after surgery. This finding is generally consistent with clinical findings, which show a decrease in SV (13, 22, 34, 39) and an increase in sphericity (12, 40) after SVR using endoventricular circular patch plasty. In contrast to what occurs after endoventricular circular patch plasty, the post-surgical LV was reported to have become more ellipsoidal when SVR was performed using septal anterior ventricular exclusion or Pacopexy technique (20). The values of SI reported here are larger than the values reported in Zhong et al. (40). This difference is because the short axis dimension was taken to be the widest LV minor axis at the endocardium based on a 4-chamber cine MRI view of the heart (40); whereas here, we have taken that dimension to be the maximum diameter of the MRI-reconstructed epicardial surface at the mid-ventricle. Our prediction that a decrease in SI can improve the diastolic and systolic function is also consistent with the theoretical studies by Choi et al. (9) and Geerts et al. (14). In these studies, an idealized prolate LV was used to show that the LV became more compliant during filling as it became more ellipsoidal (9), and the left ventricular pump function was reduced in a spherical LV when compared to an ellipsoidal LV (14). Given that the LV EDVs were smaller (around 80ml) in these studies than those found here (EDV = 176.9 ± 58 ml), the effects of sphericity appear to be size-independent, at least within the range of EDV mentioned here.

Our results show a decrease in SI by about 30% leads to an improvement in the Starling relationship of about a 3.5ml increase in SV. This result suggests that the post-surgical increase in SI contributes in part to the decrease in SV found after surgery. By restoring the LV SI back to its baseline

value (~ 30% lower than in post-surgery SI), we showed that the decrease in SV associated with an increase in sphericity cannot fully account for the 14ml post-surgical drop in SV. Therefore, it is likely that there are other mechanisms contributing to the decrease in SV other than the increased sphericity found after surgery.

Effects on myofiber stresses

Our results show that the peak end-systolic myofiber stress decreased significantly after surgery in contrast to the compromised Starling relationship. Although the bulk wall stress can be predicted using Laplace's Law, prediction of the myofiber stress and its distribution within the LV requires mathematical modeling (38). These results are therefore more accurate in predicting LV remodeling (1, 15, 32) and regional oxygen consumption (30). Our results confirm that SVR can reduce peak myofiber stress (by 50% on average), which can substantially reduce left ventricular myocardial oxygen consumption, MVO2 (30). On the other hand, myofiber stress distribution may also become more homogeneous as a result of a more uniform ventricular wall thickness after surgery (right picture in Fig. 4a). Given that left ventricular remodeling is widely believed to be initiated by an increase in both magnitude and inhomogeneity of myofiber stress (1, 15, 32), the more homogeneous myofiber stress distribution found after surgery suggests that SVR + CABG may attenuate further adverse remodeling of the LV. Whether SVR can successfully restore myofiber stress level and distribution to those found in the normal human LV and help to prevent further adverse LV remodeling will require knowledge of the myofiber stress distribution in the normal human LV.

Limitations

The limitations to our study are primarily due to the lack of acquired data. First, because MR images with delayed gadolinium enhancement were not available, infarcted regions in the LV were determined based on LV wall motion and were assumed to be transmural. As a result, other possible infarcted regions that

are less severe, particularly regions exhibiting hypokinesia, may have been omitted in our mathematical LV models.

Second, we were forced to assume physiologically reasonable values of 12 mmHg as EDP for all patients and the measured systolic blood pressure as ESP for individual patients because patient-specific left ventricular pressure data, which requires invasive measurements using micromanometer-tipped catheter, was not available. Left ventricular pressure, of course, tends to vary between patients. To overcome this limitation, we conducted sensitivity analysis to test whether our conclusions are affected by a variability in LV pressure. We have found that the conclusions are insensitive to a variation in LV pressure.

Conclusion

In this first FE analysis of the effects of CABG+SVR based on patient-specific MR images, we have quantified the global and regional functional effects resulting from geometrical changes of the LV due to surgery. The three main conclusions from our computational analysis are as follows. First, LV systolic function improved whereas LV diastolic function worsened after SVR + CABG surgery. These conflicting effects resulted in a more depressed Starling relationship after surgery. Second, post-surgical increase in LV sphericity caused the stroke volume to decrease, even though this decrease is insufficient to compensate for the drop in stroke volume found after surgery. Third, the peak myofiber stress decreased substantially (50 %) and the myofiber stress distribution became more uniform in the LV after SVR + CABG surgery. These findings are consistent with the speculation proposed in the STICH trial (20) for the neutral outcome, that "the lack of benefit seen with surgical ventricular reconstruction is that benefits anticipated from surgical reduction of left ventricular volume (reduced wall stress and improvement in systolic function) are counter-balanced by a reduction in diastolic distensibility." Since the results we presented are based on LV models reconstructed from patients at only one clinical center (Cleveland Clinic) who underwent a specific type of SVR (endoventricular circular patch plasty), they may not include the effects found when SVR is performed in other centers or when the surgery is

performed using other variants of SVR e.g., the Pacopexy technique (20), which may confer other benefits as described by Buckberg et al. (7). Since the outcome of SVR is still largely controversial, with both the European Society of Cardiology and European Association for Cardio-Thoracic Surgery recommending SVR (37) despite the negative outcome of Hypothesis 2 of the STICH trial (21), more models of other SVR variants using patient data from other clinical centers are needed to assess patient-specific efficacy of SVR.

Acknowledgement

This study was supported by the National Institutes of Health research grants: R01 HL077921 and R01 HL086400 (JMG) and R01 HL063348, R01 HL084431 (MBR) and HL-084529 (GSK). This support is gratefully acknowledged.

References

1. Aikawa Y., Rohde L., Plehn J., Greaves S.C., Menapace F., Arnold M.O., Rouleau J.L., Pfeffer M.A., Lee R.T., Solomon S.D. 2001 Regional wall stress predicts ventricular remodeling after anteroseptal myocardial infarction in the Healing and Early Afterload Reducing Trial (HEART): an echocardiography-based structural analysis. *Am. Heart J.* **141**, 234-242.

2. Aroney C.N., Herrmann H.C., Semigran M.J., William G., Boucher C.A., Fifer M.A. 1989 Linearity of the left ventricular end-systolic pressure volume relation in patients with severe heart failure. *J. Am. Coll. Cardiol.* **14**, 127-134.

3. Athanasuleas C.L, Stanley A.W.H, Buckberg G.D. 1998 Restoration of contractile function in the enlarged left ventricle by exclusion of remodeled akinetic anterior segment: surgical strategy, myocardial protection and angiographic results. *J. Card. Surg.* **13**,418–428.

4. Athanasuleas C.L., Buckberg G.D., Stanley A.W.H., Siler W., Dor V., Donato M.D., Menicanti L., Oliveria S.A., Beyersdorf F., Kron I.L. et al. 2004 Surgical ventricular restoration in the treatment of congestive heart failure due to post–infarction ventricular dilation. *J. Am. Coll. Cardiol.* **44**, 1439–1445.

5. Brinke E.A., Klautz R.J., Tulner S.A., Verwey H.F., Bax J.J., Schalij M.J., van der Wall E.E., Versteegh M.I., Dion R.A., Steendijk P. 2010 Long-term effects of surgical ventricular restoration with additional restrictive mitral annuloplasty and/or coronary artery bypass grafting on left ventricular function: Six-month follow-up by pressure-volume loops. *J. Thorac. Cardiovasc. Surg.***140**,1338-1334.

6. Bourlag B.A., Lam C.S.P., Roger V.L., Rodeheffer R.J., Redfield M.M. 2009 Contractility and ventricular systolic stiffening in hypertensive heart disease: Insights into the pathogenesis of heart failure with preserved ejection fraction. *J. Am. Coll. Cardiol.* **54**, 410 – 418.

7. Buckberg G., Athanasuleas C., Conte J. 2012 Surgical ventricular restoration for the treatment of heart failure. *Nat. Rev. Cardiol.* **9**, 703-716.

8. Buckberg G.D., Athanasuleas C.L., Wechsler A.S., Beyersdorf F., Conte J.V., Strobeck J.E. 2010 The STICH trial unravelled. *Eur. J. Heart Fail.* **12**, 1024–1027.

9. Choi. H.F., D'hooge J., Rademakers F.E., Claus P. 2010 Influence of left ventricular shape on passive filling properties and end-diastolic fiber stress and strain. *J. Biomech.* **43**, 1745–1753.

10. Dang A.B., Guccione J.M., Zhang P., Wallace A.W., Gorman R.C., Gorman J.H. 3rd, Ratcliffe M.B. 2005 Effect of ventricular size and patch stiffness in surgical anterior ventricular restoration: a finite element model study. *Ann. Thorac. Surg.* **79,** 185–193.

11. Dang A.B., Guccione J.M., Mishell J.M., Zhang P., Wallace A.W., Gorman R.C., Gorman J.H. 3rd, and Ratcliffe M.B. 2005 Akinetic myocardial infarcts must contain contracting myocytes: finite-element model study. *Am. J. Physiol. Heart Circ. Physiol.* **288**, H1844–1850.

12. Donato M.D., Sabatier M., Dor V., Gensini G.F, Toso A., Maioli M., Stanley A.W.H., Athanasuleas C., Buckberg G. 2001 Effects of the DOR procedure on left ventricular

dimension and shape and geometric correlates of mitral regurgitation one year after surgery. *J. Thorac. Cardiovasc. Surg.* **121**, 91–96.

13. Donato M.D., Fantini F., Toso A., Castelvecchio S., Menicanti L., Annest L. and Burkhoff D. 2010 Impact of surgical ventricular reconstruction on stroke volume in patients with ischemic cardiomyopathy. *J. Thorac. Cardiovasc. Surg.* **140**, 1325-1331.

14. Geerts L, Kerckhoffs R, Bovendeerd P, Arts T. 2003. Towards patient specific models of cardiac mechanics: a sensitivity study. In: *Lecture Notes in Computer Science-Functional Imaging and Modeling of the Heart, Proceedings.* Berlin-Heidelberg: Springer-Verlag, 81-90.

15. Grossman W. 1980 Cardiac hypertrophy: useful adaptation or pathologic process? *Am. J. Med.* **69**, 576–584.

16. Guccione J.M., Moonly S.M., Wallace A.W., Ratcliffe M.B. 2001 Residual stress produced by ventricular volume reduction surgery has little effect on ventricular function and mechanics: a finite element model study. *J. Thorac. Cardiovasc. Surg.* **122**, 592—599.

17. Guccione J.M., Waldman L.K., McCulloch A.D. 1993 Mechanics of active contraction in cardiac muscle: part II – cylindrical models of the systolic left ventricle. *J. Biomech. Eng*. **115**, 82–90.

18. Guccione J.M., Costa K.D., McCulloch A.D. 1995 Finite element stress analysis of left ventricular mechanics in the beating dog heart. *J. Biomechanics* **28**, 1167–1177.

19. Isomura T., Hoshino J., Fukada Y., Kitamura A., Katahira S., Kondo T., Iwasaki T., Buckberg G. from the RESTORE Group. 2011 Volume reduction rate by surgical ventricular restoration determines late outcome in ischemic cardiomyopathy. *Eur. J. Heart Fail.* **13**, 423–431.

20. Isomura T., Horii T., Suma H., Buckberg G.D. and the RESTORE Group. 2006 Septal anterior ventricular exclusion (Pacopexy) for ischemic dilated cardiomyopathy: treat form not disease. *Eur. J. Cardiothorac. Surg.* **29**, S245-250.

21. Jones R.H., Velazquez E.J., Michler R.E., Sopko G., Oh J.K., O'Connor C.M., Hill J.A., Menicanti L., Sadowski Z., Desvigne-Nickens P., et al. 2009 Coronary bypass surgery with or without surgical ventricular reconstruction. *N. Engl. J. Med*. **360**, 1705–1717.

22. Menicanti L., Castelvecchio S., Ranucci M., Frigiola A., Santambrogio C., Vincentiis C., Brankovic J., Donato M.D. 2007 Surgical therapy for ischemic heart failure: single–center experience with surgical anterior ventricular restoration. *J. Thorac. Cardiovasc. Surg.* **134**, 433–441.

23. Menicanti L. and Donato M.D. 2002 The Dor procedure: What has changed after fifteen years of clinical practice? *J Thorac. Cardiovasc. Surg.* **124**, 886-890.

24. Prucz R.B., Weiss E.S., Patel N.D., Nwakanma L.U., Baumgartner W.A., Conte J.V. 2008 Coronary artery bypass grafting with or without surgical ventricular restoration: a comparison. *Ann. Thorac. Surg*. **86**, 806–814.

25. Retzlaff B., Voss B., Albrecht W., Lange R., Hinson A.G., Sabbah H.N., Lee R.J. and Bauenrschmitt R. 2010 First in man experience with left ventricular reconstruction in patients

with systolic heart failure using a novel approach of biopolymer hydrogel implantation. *Circulation.***122**, A19753 (Abstract).

26. Rouleau J.L., Michler R.E., Velazquez E.J., Oh J.K., O'Conner C.M., Desvigne-Nickens P., Sopko G., Lee K.L., Jones R.H. The STICH trial: evidence–based conclusions. 2010 *Eur. J. Heart Fail.* **12**, 1028–1030.

27. Salati M., Pajè A., Biasi P.D., Fundaró P., Cialfi A. and Santoli C. Severe diastolic dysfunction after endoventriculoplasty. 1995 *J. Thorac. Cardiovasc. Surg.* **109**, 694-701.

28. Skelly N.W., Allen J.G., Arnaoutakis G.J., Weiss E.S., Patel N.D., Conte J.V. 2011 The impact of volume reduction on early and long-term outcomes in surgical ventricular restoration for severe heart failure. *Ann. Thorac. Surg.* **91**, 104–111.

29. Streeter Jr. D.D., Spotnitz H.M., Patel D.P., Ross Jr. J., Sonnenblick E.H. 1969 Fiber orientation in the canine left ventricle during diastole and systole. *Circ. Res.* **24**, 339–347.

30. Strauer B.E., Beer K., Heitlinger K. and Höfling B. 1977 Left ventricular systolic wall stress as a primary determinant of myocardial oxygen consumption: Comparative studies in patients with normal left ventricular function, with pressure and volume overload and coronary heart disease. *Basic Res. Cardiol.* **72**, 306-313.

31. Suga H., Sagawa K. and Shoukas A.A. 1973 Load independence of the instantaneous pressure-volume ratio of the canine left ventricle and effects of epinephrine and heart rate on the ratio. *Circ. Res.* **32**, 314-322.

32. Sutton M.G., Sharpe N. 2000 Left ventricular remodeling after myocardial infarction: pathophysiology and therapy. *Circulation* **101**, 2981-2988.

33. Sun K., Stander N., Jhun C-S., Zhang Z., Suzuki T., Wang G-Y., Saeed M., Wallace A.W., Tseng E.E., Baker A.J., Saloner D., Einstein D.R., Ratcliffe M.B., Guccione J.M. 2009 A computationally efficient formal optimization of regional myocardial contractility in a sheep with left ventricular aneurysm. *J. Biomech. Eng.***131**, 111001–1 –111001–10.

34. Tulner S.A.F., Steendijk P., Klautz R.J.M., Bax J.J., Schalij M.J., van der Wall E.E., Dion R.A.E. 2006 Surgical ventricular restoration in patients with ischemic dilated cardiomyopathy: evaluation of systolic and diastolic ventricular function, wall stress, dyssynchrony, and mechanical efficiency by pressure–volume loops. *J. Thorac. Cardiovasc. Surg.* **132**, 610–620.

35. Velazquez E.J., Lee K.L., O'Connor C.M., Oh J.K., Bonow R.O., Pohost G.M., Feldman A.M., Mark D.B., Panza J.A., Sopko G. et al. 2007 The rationale and design of the surgical treatment for ischemic heart failure (STICH) trial. *J. Thorac. Cardiovasc. Surg.* **134**, 1540–1547.

36. Walker J.C., Ratcliffe M.B., Zhang P., Wallace A.W., Fata B., Hsu E.W., Saloner D., Guccione J.M. 2005 MRI based finite element analysis of left ventricular aneursym. *Am. J. Physiol. Heart. C.* **289**, H692–700.

37. Wijns W., Kolh P., Danchin N., Di Mario C., Falk V., Folliguet T., Garg S., Huber K., James S., Knuuti J. et al. 2010 Guidelines on myocardial revascularization. *Eur. Heart J.* **31**, 2501-2555.

536 38. Yin F.C. 1982 Ventricular wall stress. *Circ. Res.* **49**, 829-842.
537
538 39. Zhong L., Sola S., Tan R.S., Le T.T., Ghista D.N., Kurra K., Navia J.L., Kassab G.S. 2009
539 Effects of surgical ventricular restoration on left ventricular contractility assessed by a novel
540 contractility index in patients with ischemic cardiomyopathy. *Am. J. Cardiol.* **103**, 674–679.
541
542 40. Zhong L., Su Y., Gobeawan L., Sola S., Tan R.S., Navia J.L., Ghista D.N., Chua T.,
543 Guccione J.M., Kassab G.S. 2011 Impact of surgical ventricular restoration on ventricular
544 shape, wall stress, and function in heart failure patients. *Am. J. Physiol. Heart Circ. Physiol.*
545 **300**, H1653–H1660.

Figure Captions

Figure 1: (a) Representative finite element LV model taken from Patient 1 pre (left) and post (right) surgery. In the pre-surgery models, dark and light regions define the infarct and the remote region, respectively. (b) Sphericity index (SI) of the 12 patients before surgery (dark color bars) and after surgery (light color bars).

Figure 2: End-diastolic pressure-volume relationship (EDPVR) and end-systolic pressure-volume relationship (ESPVR) after surgery (Patient 1). Black line: Pre-surgery. Grey line: Post-surgery. Line type indicates the pressure-volume relationships resulting from the different prescribed values of ESP and EDP. Dotted line: EDP = 4 mmHg and ESP = 90% of SBP. Solid line = 12 mmHg and ESP = SBP. Dot-dash line: EDP = 20 mmHg and ESP = 110% of SBP.

Figure 3: Representative Starling relationship from three patients showing (a) no significant changes (Patient 1), (b) worsening (Patient 2), (c) improvement after surgery (Patient 4). Dotted line: pre-surgery. Solid line: post-surgery. Bounds of the predicted Starling relationship are shown as the red region for pre-surgery and as the blue region for post-surgery. These bounds were calculated from the EDPVR and ESPVR obtained by assuming an EDP of 4 and 20mmHg and an ESP of 90% and 110% of the systolic blood pressure.

Figure 4: (a) Representative end-systolic myofiber stress distribution taken from Patient 1. The left picture shows the predicted regional myofiber stress in the pre-surgery LV. The right picture shows the stress in the more spherical post-surgery LV. (b) Peak end-systolic myofiber stress of the 12 patients before and after surgery. Black, blue and grey color bars indicate peak stress in the entire pre-surgery LV, in the pre-surgery LV's remote region and in the entire post-surgery LV, respectively. Error bars show the bounds of the peak myofiber stress when ESP was varied between 90% and 110% of the SBP.

Figure 5: (a) LV with decreasing sphericity index (SI) from left to right. The original LV of Patient 1 after surgery is shown on the left panel and the "virtually elongated" LVs are on the center and right panel. (b) Effects of LV SI on EDPVR and ESPVR. (c) The effects of LV SI on the Starling relationship. Dotted line (SI = 0.96), dashed line (SI = 0.78) and solid line (SI = 0.67).

List of figures

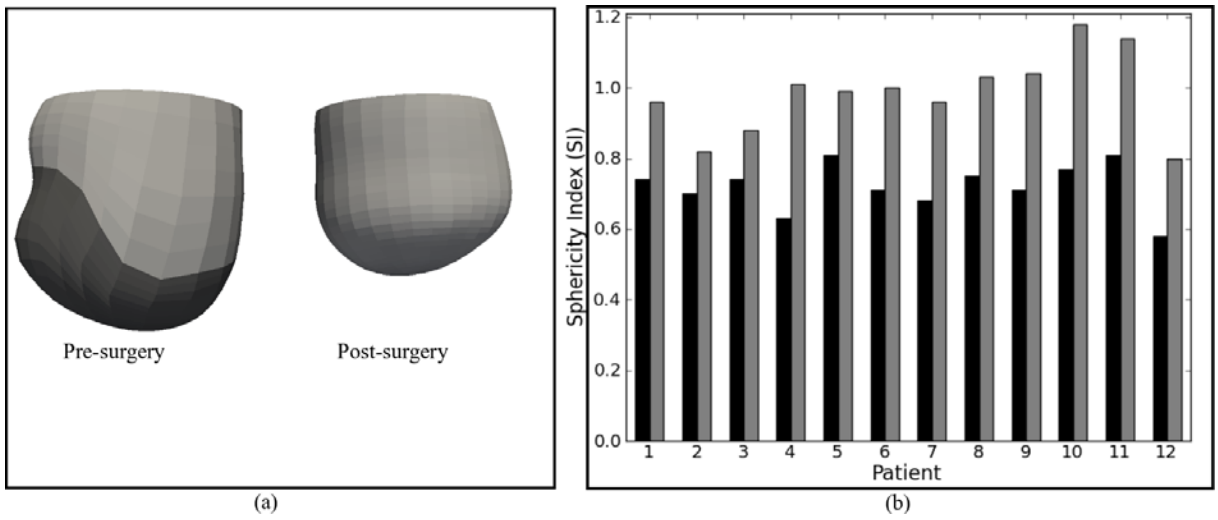

Figure 1: (a) Representative finite element LV model taken from Patient 1 pre (left) and post (right) surgery. In the pre-surgery models, dark and light regions define the infarct and the remote region, respectively. (b) Sphericity index (SI) of the 12 patients before surgery (dark color bars) and after surgery (light color bars).

585

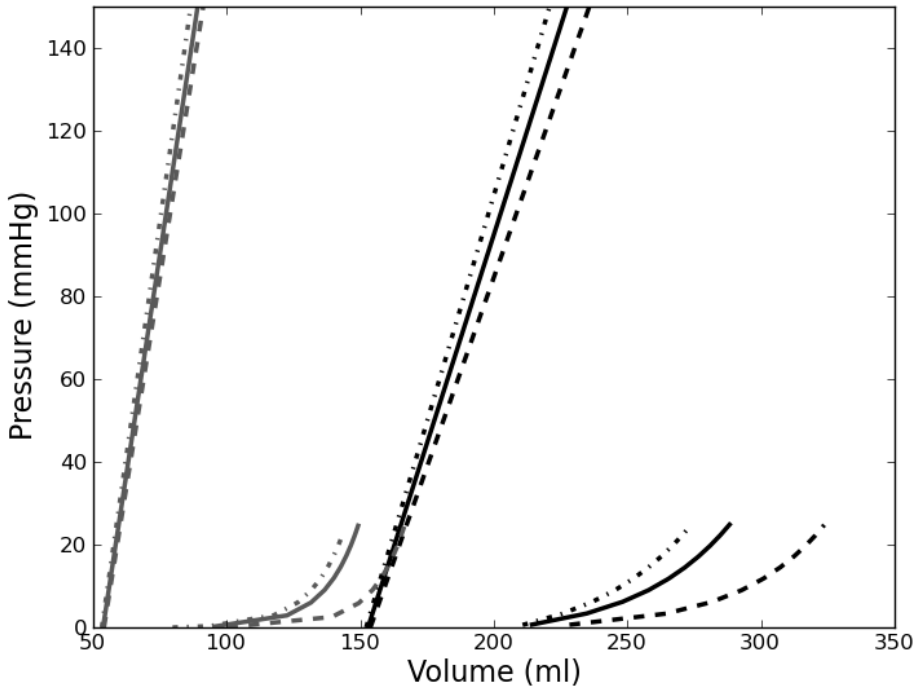

586

587 **Figure 2:** End-diastolic pressure-volume relationship (EDPVR) and end-systolic pressure-volume
588 relationship (ESPVR) after surgery (Patient 1). Black line: Pre-surgery. Grey line: Post-surgery. Line type
589 indicates the pressure-volume relationships resulting from the different prescribed values of ESP and
590 EDP. Dotted line: EDP = 4 mmHg and ESP = 90% of SBP. Solid line = 12 mmHg and ESP = SBP. Dot-
591 dash line: EDP = 20 mmHg and ESP = 110% of SBP.

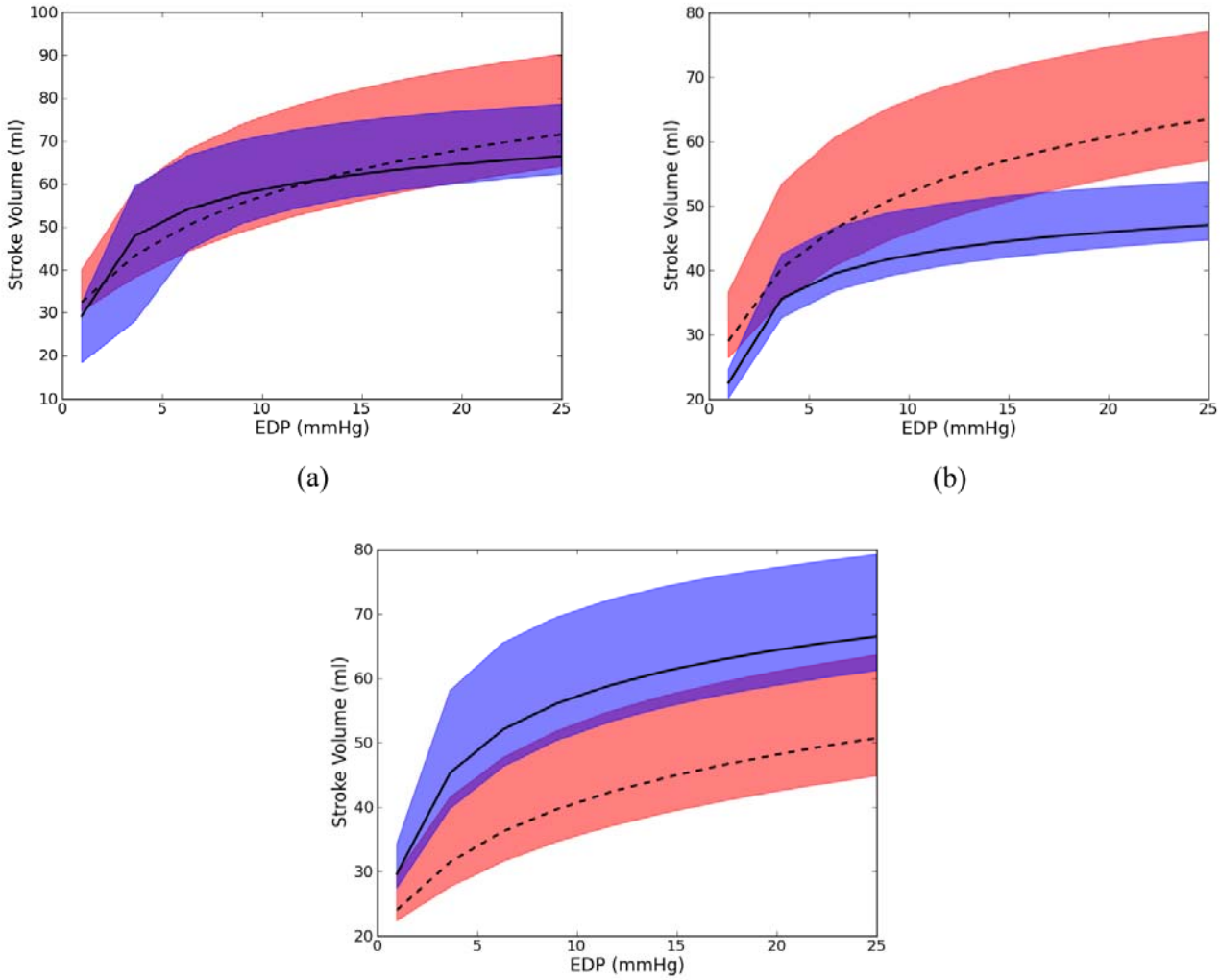

592

593 **Figure 3**: Representative Starling relationship from three patients showing (a) no significant changes
594 (Patient 1), (b) worsening (Patient 2), and (c) improvement after surgery (Patient 4). Dotted line: pre-
595 surgery. Solid line: post-surgery. Bounds of the predicted Starling relationship are shown as the red
596 region for pre-surgery and as the blue region for post-surgery. These bounds were calculated from the
597 EDPVR and ESPVR obtained by assuming an EDP of 4 and 20mmHg and an ESP of 90% and 110% of
598 the systolic blood pressure.

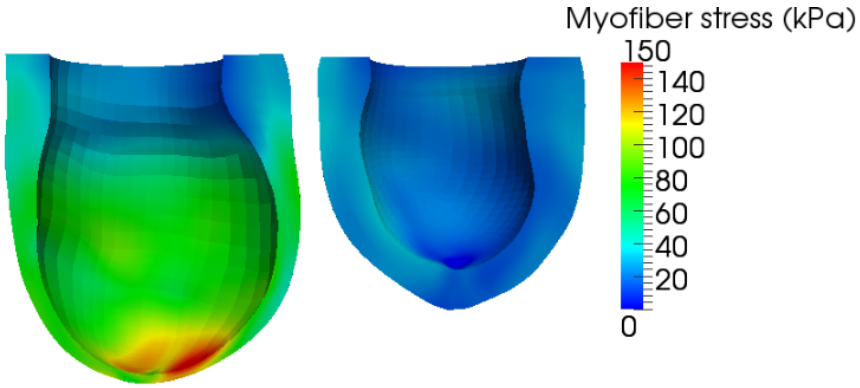

(a)

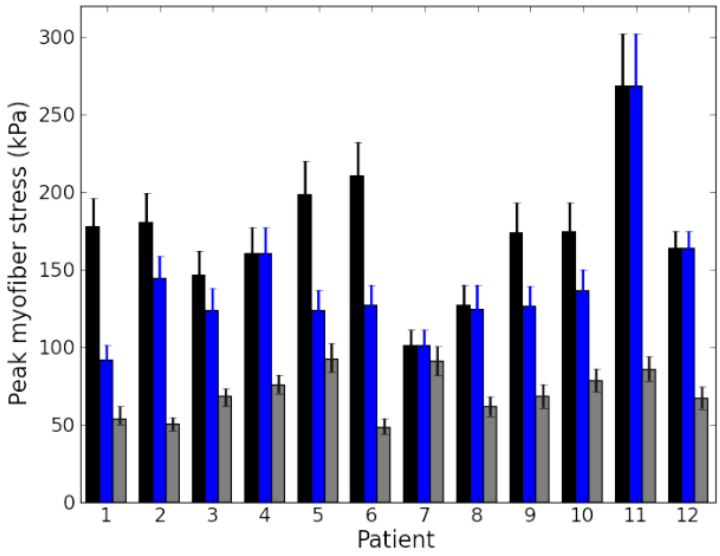

(b)

Figure 4: (a) Representative end-systolic myofiber stress distribution taken from Patient 1. The left picture shows the predicted regional myofiber stress in the pre-surgery LV. The right picture shows the stress in the more spherical post-surgery LV. (b) Peak end-systolic myofiber stress of the 12 patients before and after surgery. Black, blue and grey color bars indicate peak stress in the entire pre-surgery LV, in the pre-surgery LV's remote region and in the entire post-surgery LV, respectively. Error bars show the bounds of the peak myofiber stress when ESP was varied between 90% and 110% of the SBP.

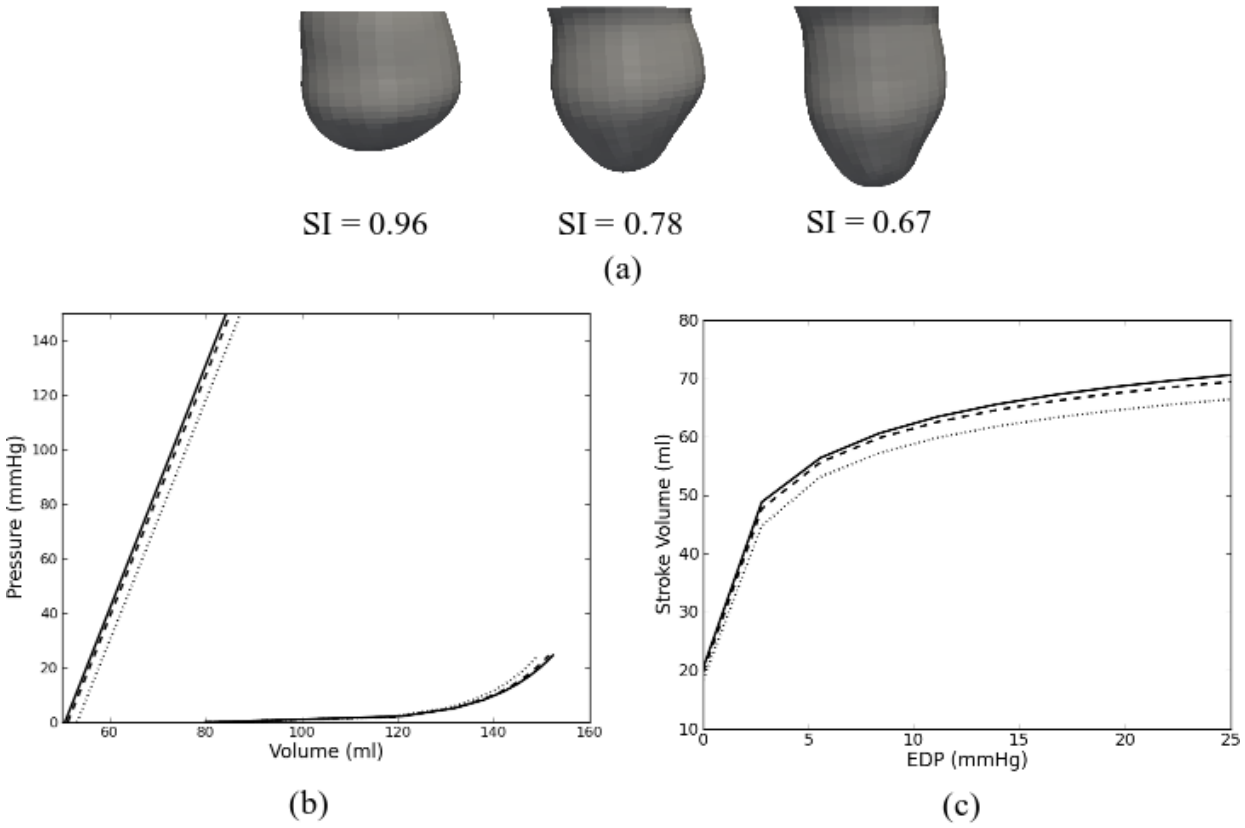

606

607 **Figure 5:** (a) LV with decreasing sphericity index (SI) from left to right. The original LV of Patient 1
608 after surgery is shown on the left panel and the "virtually elongated" LVs are on the center and right
609 panel. (b) Effects of LV SI on EDPVR and ESPVR. (c) The effects of LV SI on the Starling relationship.
610 Dotted line (SI = 0.96), dashed line (SI = 0.78) and solid line (SI = 0.67).

Appendix A.1: Constitutive law of the myocardial tissue

Nearly incompressible, transversely isotropic, hyperelastic constitutive laws for passive (18) and active myocardium (17) were used to model diastolic filling and active contraction. Passive material properties were represented by the strain energy function:

$$W = \frac{C}{2}\left\{\exp\left[b_f E_{11}^2 + b_t (E_{22}^2 + E_{33}^2 + E_{23}^2 + E_{32}^2) + b_{fs} (E_{12}^2 + E_{21}^2 + E_{13}^2 + E_{31}^2) \right] - 1 \right\}, \qquad \text{(A.1)}$$

where E_{11} is fiber strain, E_{22} is cross-fiber strain, E_{33} is radial strain, E_{23} is shear strain in the transverse plane, and E_{12} and E_{13} are shear strain in the fiber-cross fiber and fiber-radial planes, respectively. Values for the material constants b_f, b_t, and b_{fs} were obtained from large animal studies and have values 49.25, 19.25 and 17.44 respectively (33). The material constant C was adjusted until the LV end-diastolic volumes matched the experimentally measured values as described in the main text.

Active contraction was modeled by defining the total stress as the sum of the passive stress derived from the strain energy function W and an active fiber directional component, $\mathbf{T_0}$, which is a function of time, t, peak intracellular calcium concentration, Ca_0, sarcomere length, l, and maximum isometric tension achieved at the longest sarcomere length, $T_{\max}$ (17) i.e.

$$\mathbf{S} = p\, J\, \mathbf{C}^{-1} + 2\, J^{-2/3} \mathrm{Dev}\left(\frac{\partial \tilde{W}}{\partial \tilde{\mathbf{C}}}\right) + \mathbf{T}_0(t, Ca_0, l, T_{\max}), \qquad \text{(A.2)}$$

In Eq. (A.2), $\mathbf{S}$ is the second Piola-Kirchoff stress tensor, p is the hydrostatic pressure introduced as the Lagrange multiplier needed to ensure incompressibility, J is the Jacobian of the deformation gradient tensor, $\mathbf{C}$ is the right Cauchy-Green deformation tensor, $\tilde{\mathbf{C}}$ is the deviatoric decomposition of $\mathbf{C}$ (i.e. $\mathbf{C}=J^{2/3}\tilde{\mathbf{C}}$), $\tilde{W}$ is the deviatoric contribution of the strain energy function W given in Eq. (A.1) and Dev is the deviatoric projection operator defined as

$$\mathrm{Dev}(\bullet) = (\bullet) - \frac{1}{3}\left([\bullet] : \mathbf{C} \right) \mathbf{C}^{-1}. \qquad \text{(A.3)}$$

632 Assumption of near incompressibility of the myocardium also requires the decoupling of the strain energy
633 function W into its dilational U and deviatoric components $\tilde{W}$, i.e.

634 $$W = U(J) + \tilde{W}(\tilde{\mathbf{C}}). \tag{A.4}$$

635 The active fiber-directed stress component is defined by a time-varying elastance model, which at end-
636 systole, is reduced to

637 $$T_0 = \frac{1}{2} T_{\max} \frac{Ca_0^2}{Ca_0^2 + ECa_{50}^2} \left(1 - \cos\left(\frac{0.25}{m\, l_R \sqrt{2E_{11} + 1} + b} + 1\right)\pi\right). \tag{A.5}$$

638 In Eq. (A.5), m and b are material constants, and ECa_{50} is the length-dependent calcium sensitivity given
639 by

640 $$ECa_{50} = \frac{(Ca_0)_{\max}}{\sqrt{\exp\left[B\left(l_R\sqrt{2E_{11} + 1} - l_0\right)\right] - 1}}, \tag{A.6}$$

641 where B is a constant, $(Ca_0)_{\max}$ is the maximum peak intracellular calcium concentration, l_0 is the
642 sarcomere length at which no active tension develops and l_R is the stress-free sarcomere length. Material
643 constants for active contraction were taken to be (33): Ca_0 = 4.35 μmol/L, $(Ca_0)_{\max}$ = 4.35 μmol/L, B =
644 4.75 μm^{-1}, l_0 = 1.58 μm, m = 1.0489 sec μm^{-1}, b = -1.429 sec, and l_R= 1.85 μm. Based on biaxial
645 stretching experiments, cross-fiber, in-plane active stress equivalent to 40% of that along the myocardial
646 fiber direction was also added. Determination of the patient-specific material parameter $T_{\max}$ is described
647 in the main text.